Article

Structure

Structure of the RhlR-PqsE complex from *Pseudomonas aeruginosa* reveals mechanistic insights into quorum-sensing gene regulation

Graphical abstract

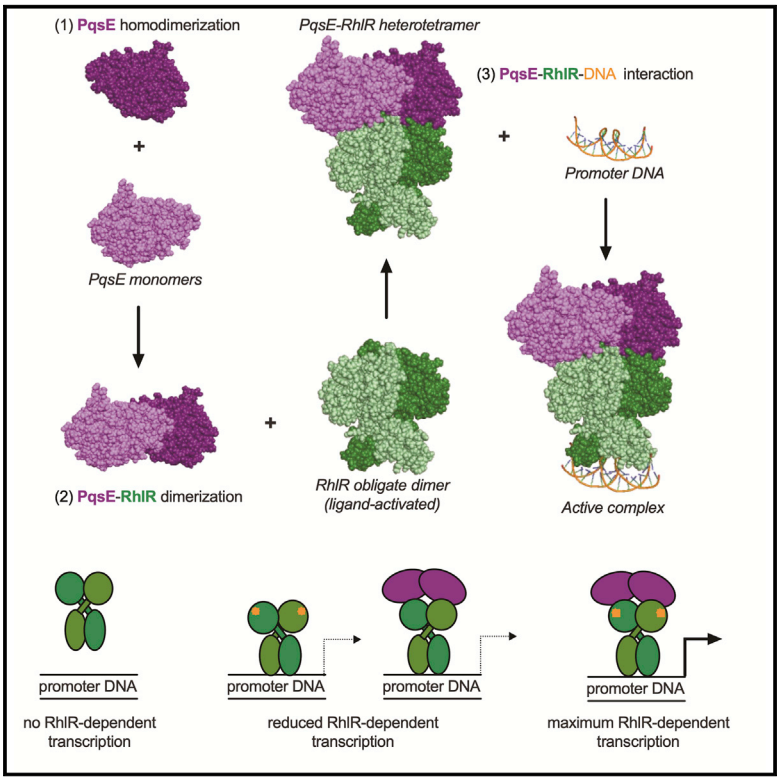

Highlights

- Virulence factor production is regulated by the RhlR-PqsE complex
- PqsE and RhlR interact via multiple interfaces to regulate RhlR DNA binding
- PqsE controls RhlR DNA binding ability by inducing RhlR to adopt an active conformation

Authors

J. Ryan Feathers, Erica K. Richael, Kayla A. Simanek, J. Christopher Fromme, Jon E. Paczkowski

Correspondence

jon.paczkowski@health.ny.gov

In brief

Feathers et al. determined the structure of the quorum-sensing receptor RhlR bound to PqsE, a complex required for pathogenesis in *Pseudomonas aeruginosa*. The structures and accompanying data established the basis for RhlR activation, providing a template for future drug discovery efforts to disrupt pathogenic signaling in *P. aeruginosa*.

Feathers et al., 2022, Structure *30*, 1–11
December 1, 2022 © 2022 Elsevier Ltd.
https://doi.org/10.1016/j.str.2022.10.008

CellPress

Please cite this article in press as: Feathers et al., Structure of the RhlR-PqsE complex from *Pseudomonas aeruginosa* reveals mechanistic insights into quorum-sensing gene regulation, Structure (2022), https://doi.org/10.1016/j.str.2022.10.008

Structure

CellPress

Article

Structure of the RhlR-PqsE complex from *Pseudomonas aeruginosa* reveals mechanistic insights into quorum-sensing gene regulation

J. Ryan Feathers,[1] Erica K. Richael,[2] Kayla A. Simanek,[3] J. Christopher Fromme,[1] and Jon E. Paczkowski[2,3,4,*]
[1]Department of Molecular Biology and Genetics, Weill Institute for Cell and Molecular Biology, Cornell University, Ithaca, NY 14853, USA
[2]Division of Genetics, Wadsworth Center, New York State Department of Health, Albany, NY 12208, USA
[3]Department of Biomedical Sciences, University at Albany, School of Public Health, Albany, NY 12201, USA
[4]Lead contact
*Correspondence: jon.paczkowski@health.ny.gov
https://doi.org/10.1016/j.str.2022.10.008

SUMMARY

Pseudomonas aeruginosa is an opportunistic pathogen that is responsible for thousands of deaths every year in the United States. *P. aeruginosa* virulence factor production is mediated by quorum sensing, a mechanism of bacterial cell-cell communication that relies on the production and detection of signal molecules called autoinducers. In *P. aeruginosa*, the transcription factor receptor RhlR is activated by a RhlI-synthesized autoinducer. We recently showed that RhlR-dependent transcription is enhanced by a physical interaction with the enzyme PqsE via increased affinity of RhlR for promoter DNA. However, the molecular basis for complex formation and how complex formation enhanced RhlR transcriptional activity remained unclear. Here, we report the structure of ligand-bound RhlR in complex with PqsE. Additionally, we determined the structure of the complex bound with DNA, revealing the mechanism by which RhlR-mediated transcription is enhanced by PqsE, thereby establishing the molecular basis for RhlR-dependent virulence factor production in *P. aeruginosa*.

INTRODUCTION

Quorum sensing (QS) is a process of bacterial cell-cell communication that controls virulence and biofilm formation in many bacterial species, including the pathogen *Pseudomonas aeruginosa*.[1,2] QS relies on the production, accumulation, detection, and population-wide response to extracellular signal molecules called autoinducers (AIs).[3–7] QS allows bacteria to synchronously alter gene-expression patterns that underpin collective behaviors, such as biofilm formation.[8]

QS progression in *P. aeruginosa* occurs in three distinct, but interconnected, waves. At the top of the QS hierarchy are two LuxI synthase/LuxR-type protein pairs that synthesize and bind acyl-homoserine lactone AIs, respectively.[9–11] LasR and RhlR detect N-(3-oxododecanoyl)-L-homoserine lactone ($3OC_{12}HSL$) and N-butyryl-L-homoserine lactone (C_4HSL), respectively.[7] $3OC_{12}HSL$ and C_4HSL are produced by the synthases LasI and RhlI, respectively. LasR and RhlR belong to a group of soluble transcription factor receptors known as LuxR-type receptors, which have a variable ligand-binding domain (LBD) and a well-conserved helix-turn-helix DNA-binding domain (DBD) (Figure 1A).[12] Upon signal recognition, LasR and RhlR activate hundreds of genes, many of which are involved in pathogenesis and the further progression of QS.[13–16]

The third QS system, termed the *Pseudomonas* Quinolone Signaling (PQS) system, is comprised of the *pqsABCDE* operon, *pqsH*, and *pqsR*. PqsABCD are responsible for the production of 4-hydroxy-2-heptylquinolone (HHQ).[17–22] PqsE functions as a metallo-β-hydrolase (Figure 1A) and is responsible for converting 2-aminobenzoylacetyl-coenzyme A (2-ABA-CoA) to 2-ABA in the PQS pathway. PqsH completes the pathway by converting HHQ to 2-heptyl-3-hydroxy-4-quinolone (PQS).[23–25] PqsR is a member of the LysR family of transcription factors and requires HHQ or PQS to function. Activated PqsR upregulates the expression of the *pqsABCDE* operon, leading to a positive feedback loop; activated PqsR upregulates the genes responsible for signal production, and the newly synthesized signal, in turn, can further activate ligand-free PqsR.[21,26] Autofeedback loops such as this are common in QS, as both LasR/LasI and RhlR/RhlI produce their respective signaling molecules using a similar mechanism. In addition to their separate regulons, LasR and RhlR co-regulate several genes, including those involved in PQS signaling.[27] LasR positively regulates the transcription of the PQS receptor (*pqsR*) and the final biosynthetic step in signal production (*pqsH*) in the PQS pathway.[13] Conversely, RhlR represses the transcription of *pqsABCDE*. Positive regulation of RhlR-dependent transcription via the PQS system was previously demonstrated.[27] The deletion of *pqsE* led to a decrease in the production of pyocyanin, an important RhlR-dependent virulence factor.[24,25] Notably, PqsE is not required to

Please cite this article in press as: Feathers et al., Structure of the RhlR-PqsE complex from *Pseudomonas aeruginosa* reveals mechanistic insights into quorum-sensing gene regulation, Structure (2022), https://doi.org/10.1016/j.str.2022.10.008

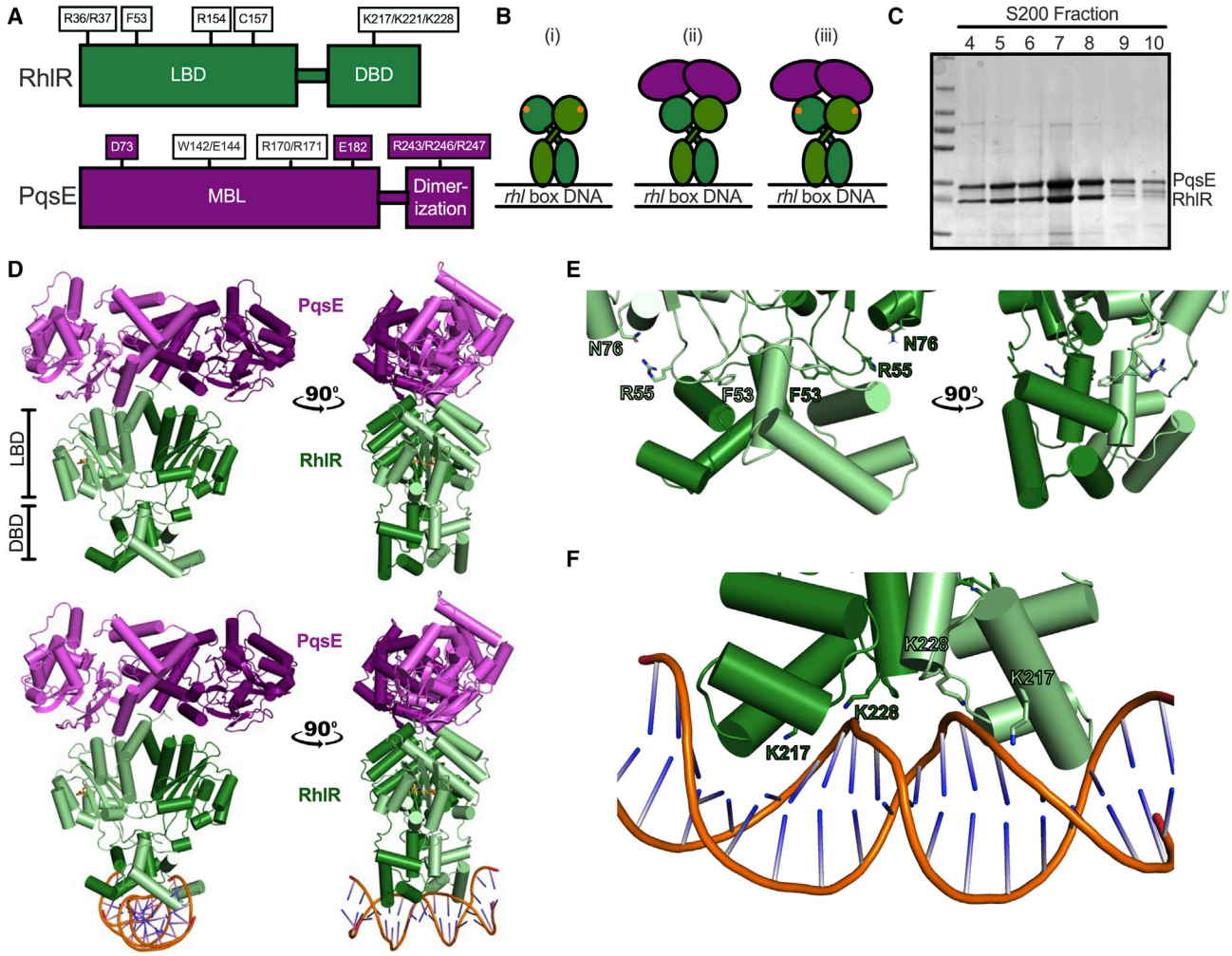

Figure 1. Structure and function of the RhlR-PqsE complex in *P. aeruginosa*

(A) Schematic of the domain architecture of RhlR and PqsE, with variants from the current study displayed in white boxes, in addition to previously characterized mutations displayed in green boxes for RhlR and purple boxes for PqsE. LBD, ligand-binding domain; DBD, DNA-binding domain; MBL, metallo-beta-lactamase domain.

(B) Schematic representation of the different mechanisms of RhlR (green) activation by C_4HSL (orange) and/or PqsE (purple).

(C) SDS-PAGE gel depicting the purified fractions from Superdex-200 size-exclusion chromatography.

(D) Structure of RhlR (green) bound to PqsE (purple) (top) or RhlR (green) bound to PqsE (purple) bound to DNA (bottom).

(E) Close-up view of the cross-domain conformation of the RhlR DBD domains. Residues F53, R55, and N76 in the RhlR LBD are highlighted.

(F) Close-up view of the cross-domain conformation of the RhlR DBD domains bound to DNA. Residues K217 and K228 in the RhlR DBD are highlighted. All structure images were created using Pymol.

See also Figures S1–S3.

produce PQS, as the loss of *pqsE* function resulted in wild-type (WT) levels of PQS. Other general thioesterases likely serve a redundant function with PqsE, resulting in the production of WT levels of PQS.[24] Curiously, insertion of a PqsE variant that was catalytically inactive on to the *P. aeruginosa* chromosome at the native *pqsE* locus produced WT levels of pyocyanin, indicating that PqsE played a role in regulating virulence outside of its proposed function in PQS biosynthesis.[28,29] We recently showed that RhlR-mediated virulence factor production is controlled by the physical interaction between PqsE and RhlR.[28] We discovered that the interaction enhances the affinity of RhlR for promoter DNA independent of the enzymatic activity of PqsE, establishing the molecular basis for PqsE regulation of RhlR function.[29]

RhlR activation by the RhlI-synthesized AI C_4HSL is not required for RhlR-dependent gene regulation as the function of RhlR can be decoupled from its partner synthase.[30,31] Transcriptional and phenotypic analyses of Δ*rhlR* and Δ*rhlI* strains revealed differences in the expression levels of certain RhlR-dependent genes and important group behaviors.[29,30,32] We showed that a Δ*rhlI* strain exhibited only modest defects in RhlR-dependent transcription compared with a Δ*rhlR* strain. For example, *hcnA* expression is regulated by RhlR independently of RhlI or the presence of C_4HSL. Furthermore, in a colony biofilm assay, a Δ*rhlI* strain formed smooth colonies, indicating the loss of biofilm matrix components, while a Δ*rhlR* strain formed hyper-rugose colonies, indicating the overproduction

Please cite this article in press as: Feathers et al., Structure of the RhlR-PqsE complex from *Pseudomonas aeruginosa* reveals mechanistic insights into quorum-sensing gene regulation, Structure (2022), https://doi.org/10.1016/j.str.2022.10.008

Table 1. Statistics for the RhlR-PqsE and RhlR-PqsE:DNA structures

	No DNA	With DNA
Nominal magnification	63,000×	
Voltage (kV)	200	
Total dose (e−/Å^2)	40	
Defocus range (μm)	−0.8 to −1.5	
Pixel size (Å)	1.29	
Symmetry imposed	C1	C1
Particle images	40,761	84,842
Map resolution, 0.143-FSC (Å)	3.74	4.10
Map sharpening B factor	−92	−125
# atoms	17,298	18,440
# protein residues	1,078	1,078
B factor, protein	18.01	33.58
RMSD, bond length (Å)	0.003	0.007
RMSD, bond angles	0.645	1.108
MolProbity score	1.83	2.03
Clash score	10.06	13.67
Poor rotamers (%)	0	0
Ramachandran favored (%)	95.61	94.30
Ramachandran allowed (%)	4.39	5.51
Ramachandran disallowed (%)	0	0.19

RMSD, root-mean-square deviation; FSC, Fourier shell correlation. Related to Figures 1 and S1–S3.

of biofilm matrix components.[30] These findings showed that decoupling of RhlI and RhlR manifests itself in the production of different group behaviors, which are regulated at the transcriptional level. Additionally, these RhlR-dependent behaviors required PqsE.[32–36] Taken together, these studies showed that RhlR-dependent transcription can proceed by multiple mechanisms. Transcription of certain genes can be induced by RhlR via activation by (1) RhlI-produced C_4HSL, (2) a physical interaction with PqsE, or (3) RhlI-produced C_4HSL and a physical interaction with PqsE (Figure 1B). Here, we determined the atomic structure of ligand-bound RhlR-PqsE and ligand-bound RhlR-PqsE:DNA complexes using single-particle cryoelectron microscopy (cryo-EM). Using structure-guided mutagenesis coupled with transcriptional analyses and phenotypic assays, we determined the structural basis for RhlR activation by PqsE, which revealed a new mechanism for transcription factor activation by an accessory protein.

RESULTS

The structure of the RhlR-PqsE complex reveals multiple binding interfaces

We co-purified the RhlR-PqsE complex by expressing untagged RhlR in the presence of the synthetic agonist meta-bromothiolactone (mBTL) and 6x-His-tagged PqsE (6x-His-PqsE) in separate strains of *Escherichia coli*.[37] Previous studies have shown that C_4HSL is not sufficient to stabilize RhlR in *E. coli* overexpression systems, necessitating the use of mBTL as the stabilizing ligand in biochemical studies.[29,37,38] We combined the soluble fractions of both lysates and purified the mixture using Ni-NTA resin followed by Superdex-200 size-exclusion chromatography (Figure 1C). We then incubated the complex with a 22-bp *rhl* box sequence at a ratio of 1:2 (protein:DNA) and performed single-particle cryo-EM analysis of the RhlR:mBTL-PqsE and RhlR:mBTL-PqsE:DNA complexes and determined the structure of both to 3.7 and 4.1 Å, respectively (Figure 1D; Table 1; Figures S1–S3). For all *in vitro* experiments, RhlR was bound by mBTL, and we omit the RhlR:mBTL nomenclature going forward. RhlR is the primary focus of the research described here. The differences and similarities with existing LuxR-type structures are addressed below.

The structure of RhlR revealed a symmetrical dimer with ~423 Å^2 of buried surface area between the LBDs (Figure 1D). The DBD is connected to the LBD by a 16-amino acid linker region. The DBD form a cross-domain conformation, resulting in the DBD of one monomer stabilized by the 11-amino acid (residues 48–58) loop region of the LBD in the opposing monomer (Figure 1E). This is mediated via hydrophobic interactions between F53 in the LBD of one monomer and α4 in the DBD in the opposing monomer. The cross-domain orientation of the DBD is further stabilized via ~675 Å^2 of buried surface area, primarily between α4 (A233 in both monomers is symmetrical) in the C terminus of the DBD (Figure 1E). The stabilized cross-domain conformation facilitates DNA binding, as α3 in the DBD of both monomers is buried in the major groove, allowing K217, K221, and K228 to interact with the phosphate backbone of DNA (Figures 1D and 1F). Presumably, this conformation is stabilized upon PqsE engagement, a point we will come to below.

The structure of PqsE was previously described; however, the structure of the RhlR-PqsE complex revealed a previously uncharacterized dimer interface for PqsE. The dimer interface also represents a point of contact with the unstructured region of the two RhlR N termini (Figure 2A), as the first 7 amino acids of RhlR are buried in a cleft formed by the PqsE dimer. PqsE residues R243, R246, and R247 were previously identified as important for RhlR-PqsE complex formation. The structure revealed that residue R243 of one monomer contacts E189 of the opposing monomer. Additionally, the PqsE dimerization interface accommodates the RhlR N termini (Figures 2A and S3A). We previously showed that substitution of all three arginine residues with alanine resulted in a disruption of the RhlR-PqsE complex. Subsequent transcriptional analysis of RhlR-dependent genes revealed this variant, which we termed PqsE-NI for "PqsE non-interacting," mimicked that of a Δ*pqsE*, indicating that the RhlR-PqsE interaction enhances RhlR-dependent signaling.[29] Thus, based on the structure of the complex, PqsE dimerization is required for complex formation, the importance of which is discussed below.

The RhlR-PqsE structure also revealed multiple additional contacts between RhlR and PqsE encompassing ~1,030 Å^2 of buried surface area. PqsE is a metallo-β-hydrolase with a αβ/αβ sandwich core structure. The second anti-parallel β-sheet forms the bulk of the interface with RhlR. Specifically, the loop region preceding β7 and the loop between β9 and β10, namely W142 and E144 and R170 and R171, respectively, form contacts with RhlR (Figures 2B and S3B). Additional hydrophobic contacts made by PqsE L213, P214,

Please cite this article in press as: Feathers et al., Structure of the RhlR-PqsE complex from *Pseudomonas aeruginosa* reveals mechanistic insights into quorum-sensing gene regulation, Structure (2022), https://doi.org/10.1016/j.str.2022.10.008

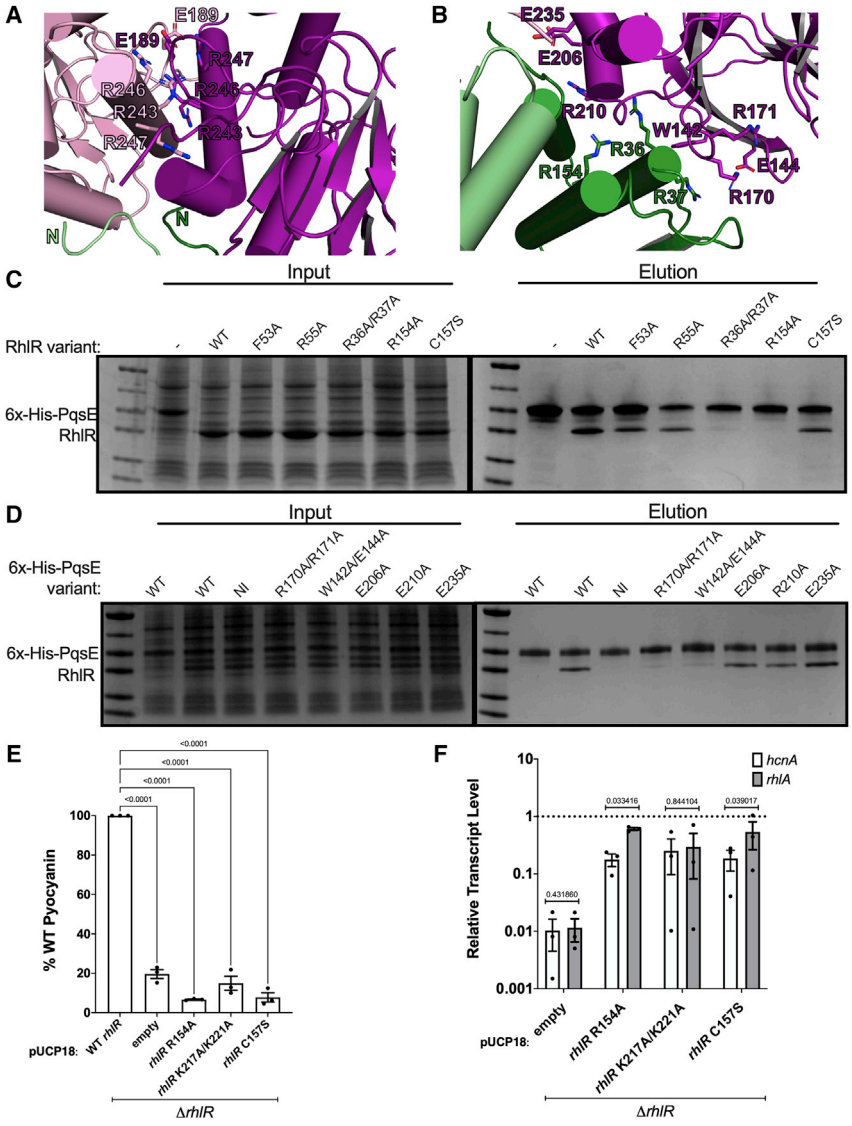

Figure 2. Characterization of the RhlR-PqsE interface and its role in RhlR-dependent signaling traits

(A) Close-up view of the N termini of RhlR (green) in the PqsE (purple) dimerization interface. Residues E189, R243, R246, and R247 (purple) in the PqsE dimerization interface are highlighted. The N- termini (green) of RhlR are labeled. All structure images were created using Pymol.

(B) Close-up view of additional contacts between RhlR (green) and PqsE (purple). Residues R36, R37, and R154 on the RhlR side (green) of the RhlR-PqsE heterodimer interface are highlighted. Residues W142, E144, R170, R171, E206, R210, and E235 on the PqsE side (purple) of the RhlR-PqsE heterodimer interface are highlighted. All structure images were created using Pymol.

(C) Affinity purification pulldown of 6x-His-PqsE with *E. coli* lysates overexpressing WT RhlR and RhlR variants hypothesized to be involved in RhlR-PqsE complex formation.

(D) As in (C) except the affinity purification pull-down was performed with WT 6x-His-PqsE and 6x-His-PqsE variants and *E. coli* lysates overexpressing WT RhlR.

(E) Pyocyanin production assay in a Δ*rhlR* strain containing empty pUCP18 plasmid or pUCP18 expressing WT RhlR or RhlR variants under the control of the *rhlR* promoter. All strains were normalized to the WT RhlR control set to 100% pyocyanin production. Three biological replicates were used, and each experiment was performed in technical duplicate. Error bars depict SEM for the biological replicates. p values were determined by performing a one-way ANOVA with a Dunnett's multiple comparisons test.

(F) qRT-PCR using the strains from (E) to measure the transcript levels of *hcnA* and *rhlA*. All strains were normalized to WT RhlR using *gyrA* as an internal housekeeping control. Three biological replicates were used, and each experiment was performed in technical duplicate. Error bars depict SEM for the biological replicates. p values were determined by performing multiple ratio paired t tests for each gene of interest within a given RhlR variant.

See also Figures S4 and S5.

L216, and L217 comprise the rest of the buried surface area with RhlR. This region of PqsE helps accommodate the N termini of the RhlR dimer that are buried in the cleft adjacent to the PqsE dimer interface (Figure 2A). Additionally, R36 and R37 in α2 and R154 in α6 in the RhlR LBD contact PqsE (Figure 2B). Due to the offset symmetry of the PqsE dimer relative to the RhlR dimer, one RhlR-PqsE dimer contributes more to the interaction interface than the second RhlR-PqsE dimer (Figure 1D). Based on our model for PqsE regulation of RhlR transcriptional activity, the RhlR variants in this study were expected to fall into one of three classes with respect to our control strains: class I is RhlR variants that mimic a Δ*pqsE* strain (i.e., can bind DNA but cannot bind PqsE), class II is RhlR variants that mimic a Δ*rhlR* strain (i.e., can bind PqsE but cannot bind DNA), and class III is RhlR variants that have intermediate activity (i.e., reduced capability to bind PqsE and/or DNA). Conversely, a PqsE variant that could not interact with RhlR was expected to mimic a Δ*pqsE* strain with respect to RhlR-dependent behaviors, as previously shown.[29]

The RhlR-PqsE complex is required to coordinate QS gene regulation and virulence factor production in *P. aeruginosa*

To confirm that the residues from the above structural analysis are important for complex formation and the activation of RhlR, we performed an affinity purification pull-down experiment. As expected, when the RhlR residues that made direct contact with PqsE in the structure were substituted with alanine, we observed a complete loss of PqsE binding, as RhlR R36A/R37A and RhlR R154A could no longer bind to PqsE (Figures 2C and S4A). The structure of the RhlR-PqsE:DNA complex revealed that K217, K221, and K228 were important for DNA binding. Indeed, RhlR K217A/K221 did not bind to promoter DNA in an electrophoretic mobility shift assay (Figure S4B). Furthermore, K217A/K221A did not exhibit a defect in binding PqsE

Please cite this article in press as: Feathers et al., Structure of the RhlR-PqsE complex from *Pseudomonas aeruginosa* reveals mechanistic insights into quorum-sensing gene regulation, Structure (2022), https://doi.org/10.1016/j.str.2022.10.008

(Figure S4C), indicating that direct binding to DNA is not a requirement for complex formation. Additional RhlR residues that were hypothesized to be important for the overall structure of the complex (i.e., stabilizing the cross-domain structure of the DBD or the RhlR dimer) had modest defects when substituted with alanine. RhlR F53A, which stabilizes the DBD in a conformation amenable to DNA binding, and RhlR C157S, which stabilizes the RhlR homodimer, bound PqsE with 50% and 70% efficacy relative to WT RhlR binding to PqsE, respectively (Figures 2C and S4A), indicating that alterations in the structure, such as disrupting the cross-domain conformation of the DBD of RhlR, can affect its ability to bind PqsE. Additionally, RhlR R55A, which was not predicted to form important contacts with PqsE but could play in a role in stabilizing the active form of RhlR, exhibited a modest, but insignificant, decrease in binding to PqsE (Figures 2C and S4A). We took an identical approach to confirm the PqsE residues most important for binding RhlR. We used PqsE-NI as a control because it was previously shown not to interact with RhlR. Consistent with the above structural analyses (Figure 2B), PqsE variants R170A/R171A and W142A/D144A did not interact with RhlR, while PqsE variants E206A, E210A, and E235A maintained binding to RhlR (Figures 2D and S4D).

To determine the role of the different interfaces in regulating virulence factor production and transcription of RhlR-dependent genes, we performed pyocyanin production assays and qRT-PCR, respectively. Analysis was focused on RhlR because RhlR variants that disrupt complex formation have not been characterized in these assays. For brevity, one RhlR variant for each of the class I (R154A), class II (K217A/K221A), and class III (C157S) variants described above was used for further analysis. For completeness, all assays were performed with one of the newly characterized PqsE variants (PqsE W142A/D144A) in addition to PqsE-NI (Figures S5A and S5B). To assess the ability of different RhlR variants to regulate virulence factor production, we performed pyocyanin production assays in a Δ*rhlR* strain containing the pUCP18 plasmid expressing *rhlR* or *rhlR* mutant alleles under the control of the native *rhlR* promoter. The ability of strains to produce pyocyanin correlated with the ability of the RhlR variant to interact with PqsE or DNA, as strains expressing all three classes of RhlR variants exhibited a significant decrease in pyocyanin production (Figure 2E). The same was true for the PqsE W142A/D144A variant that did not interact with RhlR (Figure S5A). Taken together, these results established the role of different contacts within RhlR necessary for activation and further support the model that the RhlR-PqsE interaction is required for virulence factor production.

To assess the role of the different interfaces in the RhlR-PqsE structure on RhlR-dependent transcription, we performed qRT-PCR and measured the transcript levels of *hcnA* and *rhlA* in the same strains from the pyocyanin production assay (Figures 2F and S5B). We used Δ*pqsE*, Δ*rhlR*, and PqsE-NI strains as controls. *hcnA* and *rhlA* were chosen because they have different PqsE dependencies for their expression, as RhlR is more dependent on PqsE to control *hcnA* expression compared with *rhlA*, which is regulated by RhlR with less dependence on PqsE. Thus, if a RhlR variant was defective in PqsE binding, DNA binding, or both, it could be determined based on the relative transcript levels of the two different genes within a single strain. For example, *hcnA* expression compared with *rhlA* expression would be disproportionately affected in a strain containing a RhlR variant that cannot interact with PqsE but maintained DNA binding, and the relative transcript levels for *hcnA* would be lower than that of *rhlA*. Conversely, a RhlR variant that is deficient in DNA binding or deficient in both DNA and PqsE binding should exhibit no difference between *hcnA* and *rhlA* expression because these classes of variants are generally disruptive of RhlR function. Indeed, these trends were observed as the strain expressing RhlR R154A (class I) exhibited a 3-fold difference in the relative transcript levels of *hcnA* and *rhlA*, while a strain expressing RhlR K217A/K221A (class II) displayed no difference in the relative transcript levels of *hcnA* and *rhlA* (Figure 2F).

The structure of the RhlR-PqsE complex is unique within the context of QS gene regulation

One of closest homologs of RhlR is SdiA from *Enterobacter* spp. (Figure S6). SdiA, characterized in both *E. coli* and *Salmonella enterica*, is a unique receptor because it has no known cognate AI synthase to produce HSL, and its role as a QS receptor is less clear compared with LuxR-type proteins from other well-characterized systems. Nonetheless, the structure of SdiA bound to $3OC_8$HSL was solved, and the structure is nearly superimposable with the structure of RhlR[39] (Figure 3A). It was hypothesized that the structure of SdiA represented the activated form of the receptor, primed to bind to DNA. The structures presented here indicate that this is likely the case, as RhlR bound and unbound by DNA adopted a similar conformation. However, the structure of RhlR bound to DNA is distinct from the only other structure of a LuxR-type protein bound to DNA: TraR bound to its AI $3OC_8$HSL from *Agrobacterium tumefaciens*. The structure of TraR bound to an 18-bp fragment of the *tra* box revealed an asymmetry in the DBD relative to the DNA (Figure 3A), resulting in one monomer being more elongated than its partnered monomer.[40] The authors hypothesized that this was due to the relatively long, flexible linker region connecting the LBD with the DBD and that this conformation was important for additional proteins to bind TraR to activate transcription. However, similar asymmetry is not observed in our structure of RhlR bound to DNA (Figures 1D and 3A), suggesting that these two related receptors may have evolved divergent mechanisms for activation by other proteins. Indeed, *A. tumefaciens* does not contain a PqsE homolog and likely uses a different mechanism for initiating its QS pathways via TraR.

To determine the molecular basis for the specificity of PqsE for RhlR, we built an *E. coli* reporter system expressing LasR, the other LuxR-type receptor found in *P. aeruginosa*, under the control of an arabinose promoter in the presence of the *lasB* promoter fused to *luxCDABE* with or without PqsE constitutively expressed under the *lac* promoter. This is similar to the *E. coli* reporter system we previously used to assess RhlR function in the presence or absence of PqsE.[29] PqsE expression had no effect on the ability of LasR to regulate the *lasB* promoter (Figure 3B), indicating that even within the *P. aeruginosa* QS network, PqsE is specific for RhlR activation. To determine how the RhlR-PqsE interaction could have evolved specificity for RhlR, we performed a conservation analysis coupled to structural analysis using the ConSurf server.[42–45] In Figure 3C, the most conserved (red) and the most variable (blue) residues in RhlR based on

Please cite this article in press as: Feathers et al., Structure of the RhlR-PqsE complex from *Pseudomonas aeruginosa* reveals mechanistic insights into quorum-sensing gene regulation, Structure (2022), https://doi.org/10.1016/j.str.2022.10.008

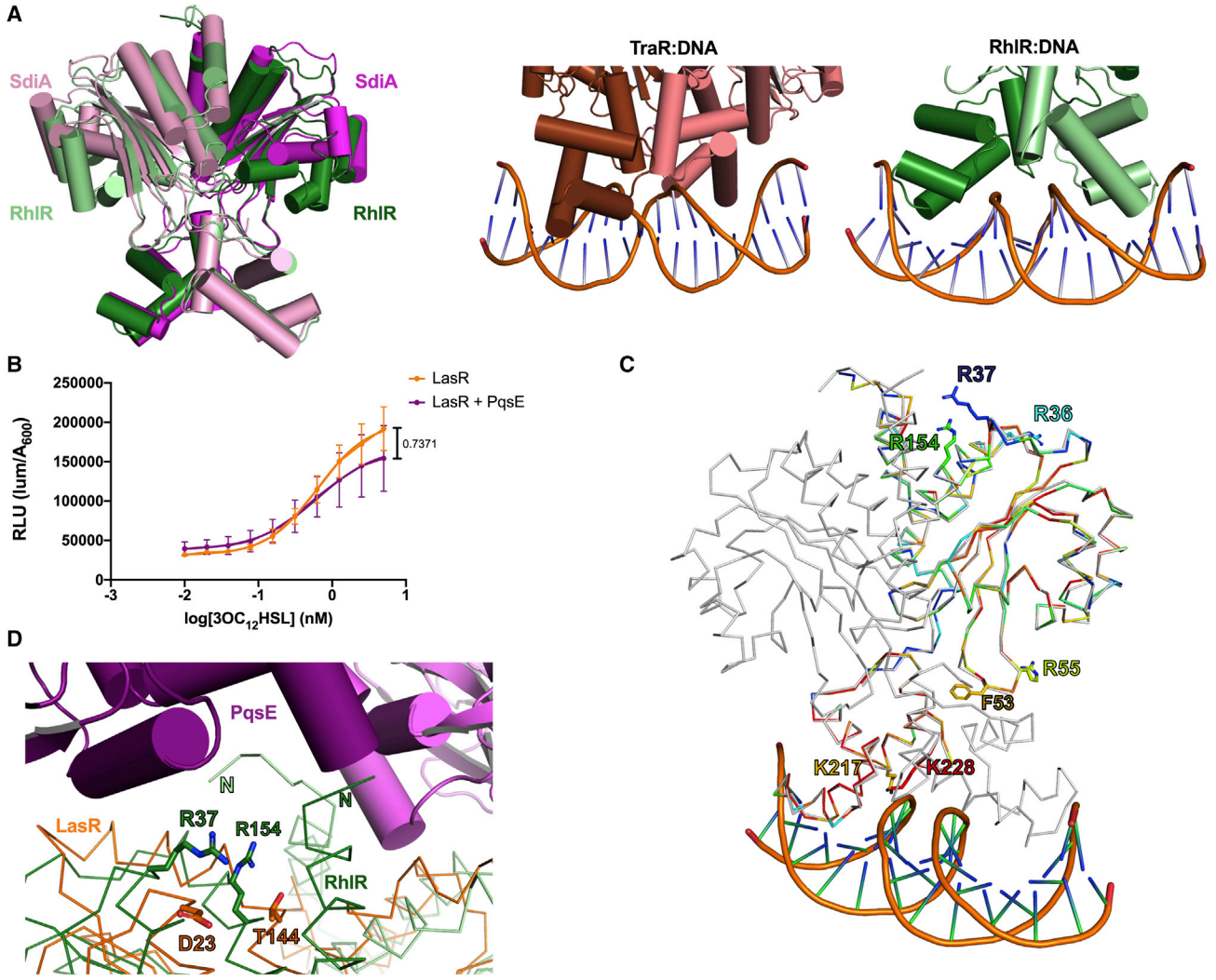

Figure 3. Contextualizing the RhlR-PqsE interaction in QS

(A) (Left) Overlay of the structures of SdiA (pink; PDB: 4LFU[39]) and RhlR (green) and (right) comparison of the DBD of TraR (brown; PDB: 1H0M[40]) and RhlR (green) bound to their respective *tra* or *rhl* boxes.

(B) *E. coli* reporter assay expressing LasR under the control of the pBAD promoter in the presence of the *lasB* promoter fused to *luxCDABE* with (purple) or without (orange) constitutively expressed PqsE. The assay was performed in a 10-point dose response with 2-fold serial dilutions. The top concentration of $3OC_{12}HSL$ was 2 nM. Three biological replicates were used, and each experiment was performed in technical duplicate. Error bars depict SEM. RLU, relative light units. A non-linear regression analysis was performed for each of the curves, and a p value was assigned based on differences in the calculated half-maximal effective concentration (EC_{50}) value.

(C) Ribbon diagram depicting the conservation analysis of RhlR compared with 150 LuxR-type receptors. One monomer is colored in rainbow based on conservation scores from ConSurf analysis shown in Table S1, and the other monomer is colored gray for clarity. Red residues are highly conserved, and blue residues are highly variable amongst the 150 homologs analyzed. PqsE is omitted for clarity.

(D) Overlay of the structure of LasR (orange; PDB: 6MWL[41]) with RhlR (green) at the PqsE (purple) interface. Residues D23 and T144 in LasR (orange) and residue R37 and R154 in RhlR (green) are highlighted. LasR and RhlR are depicted as ribbons for clarity of the overlaid structures. All structure images were created using Pymol.

See also Figure S6 and Table S1.

alignment with 150 LuxR-type receptors are shown (Table S1). The residues in RhlR that were essential for RhlR-PqsE complex formation in Figure 2C were some of the least conserved residues in RhlR relative to the other 150 LuxR-type receptors (Figure 3C; Table S1), indicating that this region of the protein is not conserved likely due to its highly specific function in *P. aeruginosa* and other closely related species. Indeed, the presence of *pqsE* is largely confined to the *Pseudomonas* and *Burkholderia* genera with a few exceptions. Within *P. aeruginosa*, the interaction is highly specific; when we compared the structures of RhlR and LasR, we found that R37 and R154 in RhlR corresponded to D23 and T144 in LasR, respectively (Figure 3D).[41] The nature of the side chains and the interactions they can form dictates if a receptor can bind PqsE. Therefore, RhlR can interact with PqsE and LasR cannot. Thus, these structural analyses establish the molecular basis for

Please cite this article in press as: Feathers et al., Structure of the RhlR-PqsE complex from *Pseudomonas aeruginosa* reveals mechanistic insights into quorum-sensing gene regulation, Structure (2022), https://doi.org/10.1016/j.str.2022.10.008

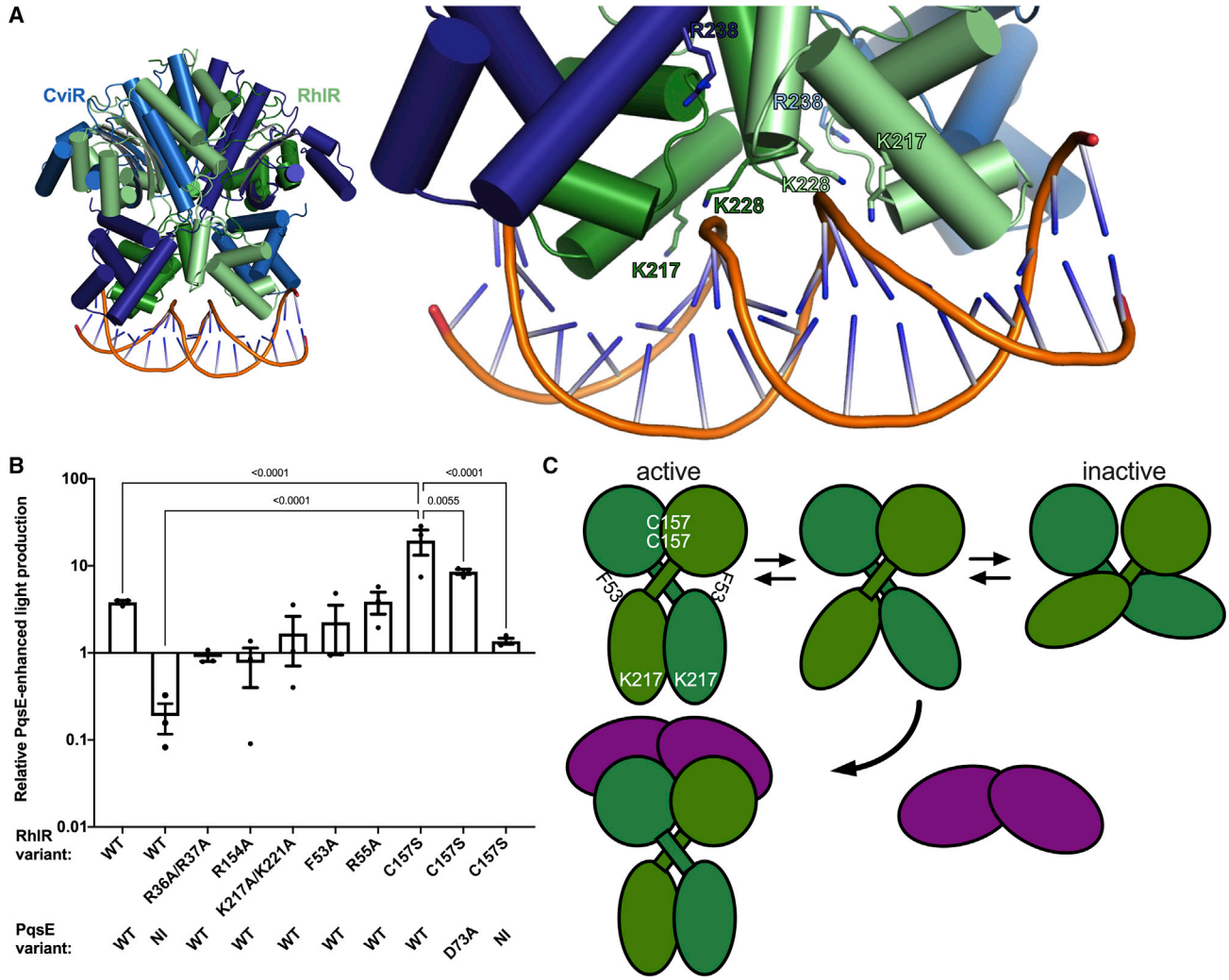

Figure 4. Structural basis for PqsE-induced RhlR activation

(A) Comparison of the closed, inhibited conformation structure of CviR (blue; PDB: 3QP6[46]) bound to the antagonist CL and the open, activated conformation of RhlR (green) bound to the agonist mBTL, PqsE, and DNA. Residue R238 in CviR (blue) and residues K217 and K228 in RhlR (green) are highlighted to display the structural changes between the closed and active states of LuxR-type proteins. All structure images were created using Pymol.

(B) *E. coli* reporter assay expressing RhlR or RhlR variants under the control of the pBAD promoter in the presence of the *rhlA* promoter fused to luciferase with or without constitutively expressed PqsE. Light levels were normalized to their respective control strain lacking PqsE for each variant. Three biological replicates were used, and each experiment was performed in technical duplicate. Error bars depict SEM for the biological replicates. p values were determined by performing a one-way ANOVA with a Dunnett's multiple comparisons test. Comparisons are only shown relative to the RhlR C157S variant for simplicity.

(C) Cartoon model for RhlR activation by PqsE.

See also Figure S7.

the specificity of the RhlR-PqsE interaction as well as provide insights into how the interaction could have evolved.

The structure of the RhlR-PqsE:DNA complex reveals the molecular basis for RhlR activation

Previous structures of other LuxR-type receptors have revealed remarkable flexibility at the linker region joining the N-terminal LBD and the C-terminal DBD.[40,46] The structure of CviR from *Chromobacterium violaceum* bound to the inhibitor chlorolactone (CL) revealed a closed conformation that locked the helices of the DBD in an orientation that could no longer bind DNA (Figure 4A).[46] RhlR K217 corresponds to R238 in its homolog CviR. The comparison of the structures of inhibited CviR and activated RhlR revealed a distance of 43.5 Å between CviR R238 and RhlR K217, consistent with the hypothesis that the DBD can sample multiple conformations and that the collective structural data are snapshots of the receptors occupying the two most stable states (i.e., either open/bound to DNA [active] or closed [inactive]) (Figure 4A). We hypothesize that RhlR adopts multiple conformations with respect to its DBD and that PqsE provides the structural rigidity for adopting the active, high-affinity state for DNA binding, as PqsE binding the RhlR LBD locks the DBD in a fixed, cross-domain conformation.

Please cite this article in press as: Feathers et al., Structure of the RhlR-PqsE complex from *Pseudomonas aeruginosa* reveals mechanistic insights into quorum-sensing gene regulation, Structure (2022), https://doi.org/10.1016/j.str.2022.10.008

To determine the molecular basis for PqsE-dependent RhlR activation, we compared the structure of the RhlR-PqsE complex with that of the RhlR-PqsE complex bound to DNA. The structure of the RhlR-PqsE complex unbound to DNA is identical in structure to that of the RhlR-PqsE complex bound to DNA (Figure 1D). These findings support the notion that RhlR bound by PqsE is primed for binding DNA. To understand how the structure of RhlR might be altered when bound by PqsE, we used RhlR variants with defects in binding to PqsE in an *E. coli* reporter system that expresses *rhlR* and *rhlR* mutant alleles under the control of an arabinose-inducible promoter in the presence of a second plasmid containing the promoter of *rhlA* fused to *luxCDABE* (luciferase). Each strain, expressing *rhlR* or the *rhlR* mutant allele, contained either an empty control plasmid or a plasmid constitutively expressing *pqsE*. Given that each of the variants had different baseline reporter expression levels compared with WT RhlR, due to alterations in the structure of RhlR (Figure S7), the effects of PqsE expression on each RhlR variant was normalized to its control strain harboring an empty plasmid. In RhlR variants that cannot bind PqsE, we did not expect an increase in light production because PqsE-dependent enhancement of transcription cannot occur (Figure 4B). Indeed, expression of WT PqsE enhanced RhlR-dependent light production by ~4-fold in the strain expressing WT RhlR, while PqsE did not enhance RhlR-dependent light production in strains expressing RhlR R36A/R37A or R154A, similar to when PqsE-NI was expressed with WT RhlR (Figure 4A), thus confirming the role of these interfaces in RhlR-PqsE complex formation. In RhlR variants that could not bind DNA but could bind to PqsE, we did not expect an increase in light production because RhlR must bind to promoter DNA for PqsE-dependent enhancement of RhlR-dependent transcription to occur. As expected, expression of WT PqsE did not enhance RhlR-dependent light production in a strain expressing RhlR K217A/K221A (Figure 4B).

The above analyses used RhlR variants that were incapable of binding PqsE or DNA (class I and class II variants), and, as expected, RhlR-dependent transcription of the reporter could not be enhanced by PqsE. To determine the structural basis for PqsE activation of RhlR, the RhlR variants F53A, R55A, and C157S that exhibited modest defects in binding PqsE were included in the assay (Figure 2C). We surmised that the variants could be used to determine the role of different points of contact within the complex in controlling RhlR function and, in turn, determine how PqsE can alter RhlR structure. RhlR F53 and R55, which are important for stabilizing the cross-domain conformation of the DBD, still bound PqsE when substituted with alanine, albeit with reduced efficacy compared with WT RhlR (Figure 2C). However, both variants were incapable of inducing reporter expression in the light assay (Figure S6), indicating that the RhlR variants were defective in adopting the cross-domain conformation, resulting in an ability to bind DNA. Additionally, this defect could not be rescued by overexpression by PqsE (Figure 4B), indicating that these variants are likely defective not only in binding PqsE but also in adopting a conformation amenable to binding DNA. The cross-domain conformation is stabilized via an interaction of the RhlR LBD loop region, consisting of residues 48–58, and the α-helices in the DBD (Figure 1E), and the loss of this stabilization via substituting F53 or R55 with alanine renders the complex non-functional.

The most dramatic effect of PqsE expression on RhlR-dependent expression of the reporter was observed with the RhlR C157S variant. We hypothesized that the C157S substitution disrupted the hydrophobic core of the dimer interface, likely leading to a disruption of the RhlR dimer interface and resulting in a loss of RhlR-dependent transcription. Indeed, without PqsE present, the strain expressing RhlR C157S produced ~30-fold less light compared with WT RhlR without PqsE (Figure S7). Notably, compared with RhlR F53A and RhlR R55A, RhlR C157S could still function as a transcriptional activator, and we hypothesized that RhlR C157S could be rescued by PqsE expression. Indeed, expression of PqsE partially rescued the destabilization of the RhlR dimer and restored the functional tetramer, as evidenced by the ~19-fold enhancement in light production when PqsE was expressed (Figure 4B). To further characterize the nature of enhanced RhlR transcription by PqsE in the RhlR C157S variant, two previously characterized PqsE variants, PqsE-NI and PqsE D73A, were co-expressed with RhlR C157S in the *E. coli* reporter system. The PqsE-NI variant disrupted the PqsE dimerization interface and abolished the PqsE interaction with RhlR. The PqsE D73A variant was characterized as a catalytically inactive variant that could still bind and regulate RhlR. The co-expression of RhlR C157S with PqsE D73A resulted in an ~12-fold increase in light production compared with a strain expressing RhlR C157S in the absence of WT PqsE (Figure 4B). Conversely, PqsE-NI could not restore RhlR C157S function, and light levels did not increase compared with a strain expressing RhlR C157S without PqsE. In total, the RhlR C157S variant could not fully interact with RhlR (Figure 2C), which resulted in decreased pyocyanin production (Figure 2E) and decreased transcription of *hcnA* and *rhlA* to varying degrees (Figure 2F). These differences are likely the result of the varying dependences for RhlR-dependent gene regulation on PqsE (see discussion).[29] Indeed, RhlR C157S had diminished activity on its own in the light assay (Figure S7), which could be recovered only by the overexpression of WT PqsE or PqsE D73A and not PqsE-NI, supporting the model that PqsE can stabilize a RhlR dimer to adopt a conformation amenable to binding DNA (Figure 4C).

DISCUSSION

The RhlR-PqsE complex and its role in activating RhlR-dependent transcription is unique in the field of QS and, more generally, in the field of prokaryotic transcription. We are not aware of any such instances in which a QS transcription factor receptor requires an additional protein to optimally bind promoter DNA and initiate target gene expression.[29] The closest analogous mechanism in bacteria is the role of sigma factors in directing transcription factors to certain promoters.[47] However, this function of sigma factors is sequence specific as they also bind promoter DNA, while PqsE does not.[29]

Previously published RNA sequencing (RNA-seq) experiments showed a stronger PqsE dependency for certain RhlR-regulated genes than others. While the structures revealed the general mechanism of activation for RhlR by PqsE, the molecular basis for promoter specificity and PqsE dependency is not immediately clear. We hypothesize that RhlR bound by PqsE adopts a conformation that generally enhances its affinity for promoter DNA while driving RhlR to certain low-affinity promoters that it

Please cite this article in press as: Feathers et al., Structure of the RhlR-PqsE complex from *Pseudomonas aeruginosa* reveals mechanistic insights into quorum-sensing gene regulation, Structure (2022), https://doi.org/10.1016/j.str.2022.10.008

cannot otherwise regulate without PqsE. Genome-wide DNA binding analyses for RhlR and RhlR-PqsE will reveal the molecular basis for PqsE dependency at certain promoters. Identifying the promoters most dependent on PqsE for RhlR binding will be important to determining how certain RhlR-dependent genes and phenotypes are regulated. It is not yet known if all RhlR in the cell is bound by PqsE or what the regulatory mechanisms are that drive RhlR-PqsE complex formation. All these factors will need to be considered when assessing QS progression, especially within the context of infection. *pqsE* and *rhlR* are rarely mutated in *P. aeruginosa* clinical isolates, and no such variants that would disrupt RhlR-PqsE complex formation have been identified in the publicly available strain databases. Thus, we hypothesize that RhlR-PqsE complex formation is a critical step in pathogenesis signaling and disease progression.

Related to the role of the RhlR-PqsE complex formation in pathogenesis, previous work on PqsE discovered two important factors that make it an ideal candidate for drug discovery: (1) the RhlR-PqsE interaction is required for lung colonization in a murine model, and (2) PqsE variants that mimic the inhibitor bound state in the catalytic pocket of PqsE disrupted its ability to bind RhlR.[28,48] Targeting QS-dependent group behaviors has long been thought of as a viable alternative or supplement to traditional bactericidal or bacteriostatic treatments because it would reduce the selective pressures that give rise to antibiotic resistance while suppressing important virulence traits. The structure of the complex revealed the possible mechanism of action for targeting the PqsE catalytic pocket with a small-molecule inhibitor and how this can lead to a disruption of the RhlR-PqsE interaction and, thus, virulence factor production *in vivo*. Specifically, PqsE function was abrogated, both catalytically and in its ability to interact with RhlR, when residue E182 was substituted with a tryptophan.[28] E182 is buried in the catalytic pocket in a long flexible loop region that structurally links the catalytic domain with the newly discovered dimerization interface in PqsE (Figure 1A). Part of this loop region, comprised of residues 187–191, forms an interaction surface with the long α-helix containing residues R243, R246, and R247 that were previously shown to be important for complex formation and, as shown in Figure 2A, are important for PqsE homodimerization. We hypothesize that substituting E182 with a tryptophan leads to a structural change in the loop region that results in a perturbation of the α-helix in the opposing monomer, leading to a dissociation of the PqsE dimer and, as prior work would indicate, blocking the interaction between RhlR and PqsE. Thus, the RhlR-PqsE complex has multiple potential target sites for small-molecule inhibition. This can occur allosterically through the catalytic pocket or via the direct interfaces between RhlR and PqsE. While there is a precedence for the former mechanism, no effort has been made to directly disrupt the RhlR-PqsE complex from forming.[2] The structures reported here provide a comprehensive guide to do both.

STAR★METHODS

Detailed methods are provided in the online version of this paper and include the following:

- KEY RESOURCES TABLE
- RESOURCE AVAILABILITY
  - Lead contact
  - Materials availability
  - Data and code availability
- EXPERIMENTAL MODEL AND SUBJECT DETAILS
- METHOD DETAILS
  - Plasmid and strain construction
  - Affinity purification pulldown
  - *E. coli* light assay
  - Pyocyanin production assay
  - RNA extraction and qRT-PCR
  - Protein purification and cryo-EM sample preparation
  - Imaging conditions
  - Data processing
  - Model building
- QUANTIFICATION AND STATISTICAL ANALYSIS

SUPPLEMENTAL INFORMATION

Supplemental information can be found online at https://doi.org/10.1016/j.str.2022.10.008.

ACKNOWLEDGMENTS

The authors thank Drs. Bonnie Bassler and Isabelle Taylor for providing their feedback on the research. The authors thank the research laboratories in the Division of Genetics at the Wadsworth Center, New York State Department of Health, for helpful discussions on the research and for resource sharing. We thank the dedicated staff scientists at the CCMR at Cornell University and the Advanced Genomics Technologies Center and Media & Tissue Core facilities at the Wadsworth Center, New York State Department of Health. This work was supported by National Institutes of Health grant 1R01GM14436101, New York Community Trust Foundation grant P19-000454, and Cystic Fibrosis Foundation grant PACZKO21G0 to J.E.P, NIH grant R35GM136258 to J.C.F., and a Ford Foundation Fellowship to J.R.F. The Cornell Center for Materials Research (CCMR) is supported by NSF grant DMR-1719875.

AUTHOR CONTRIBUTIONS

Conceptualization, J.R.F., J.C.F., and J.E.P.; methodology, J.R.F., J.C.F., and J.E.P.; investigation, J.R.F., E.K.R., and K.A.S.; writing – original draft, J.R.F., E.K.R., K.A.S., J.C.F., and J.E.P.; writing – review & editing, J.R.F., E.K.R., K.A.S., J.C.F., and J.E.P.; funding acquisition, J.C.F. and J.E.P.; resources, J.R.F., E.K.R., and K.A.S.; supervision, J.C.F. and J.E.P.

DECLARATION OF INTERESTS

The authors declare that they have no conflicts of interest with the contents of this article. The content is solely the responsibility of the authors and does necessarily represent the official views of the National Institutes of Health. The funders had no role in study design, data collection and analysis, decision to publish, or preparation of the manuscript.

INCLUSION AND DIVERSITY

One or more of the authors of this paper self-identifies as an underrepresented ethnic minority in science. One or more of the authors of this paper self-identifies as a member of the LGBTQ+ community. One or more of the authors of this paper received support from a program designed to increase minority representation in science. We support inclusive, diverse, and equitable conduct of research.

Received: August 3, 2022
Revised: August 26, 2022
Accepted: October 20, 2022
Published: November 14, 2022

Please cite this article in press as: Feathers et al., Structure of the RhlR-PqsE complex from *Pseudomonas aeruginosa* reveals mechanistic insights into quorum-sensing gene regulation, Structure (2022), https://doi.org/10.1016/j.str.2022.10.008

REFERENCES

1. Papenfort, K., and Bassler, B.L. (2016). Quorum sensing signal-response systems in Gram-negative bacteria. Nat. Rev. Microbiol. *14*, 576–588.
2. Simanek, K.A., and Paczkowski, J.E. (2022). Resistance is not futile: the role of quorum sensing plasticity in *Pseudomonas aeruginosa* infections and its link to intrinsic mechanisms of antibiotic resistance. Microorganisms *10*, 1247.
3. Engebrecht, J., Nealson, K., and Silverman, M. (1983). Bacterial bioluminescence: isolation and genetic analysis of functions from *Vibrio fischeri*. Cell *32*, 773–781.
4. Bassler, B.L., Wright, M., and Silverman, M.R. (1994). Sequence and function of LuxO, a negative regulator of luminescence in *Vibrio harveyi*. Mol. Microbiol. *12*, 403–412.
5. Gambello, M.J., and Iglewski, B.H. (1991). Cloning and characterization of the *Pseudomonas aeruginosa lasR* gene, a transcriptional activator of elastase expression. J. Bacteriol. *173*, 3000–3009.
6. Seed, P.C., Passador, L., and Iglewski, B.H. (1995). Activation of the *Pseudomonas aeruginosa lasI* gene by LasR and the *Pseudomonas* autoinducer PAI: an autoinduction regulatory hierarchy. J. Bacteriol. *177*, 654–659.
7. Latifi, A., Winson, M.K., Foglino, M., Bycroft, B.W., Stewart, G.S., Lazdunski, A., and Williams, P. (1995). Multiple homologues of LuxR and LuxI control expression of virulence determinants and secondary metabolites through quorum sensing in *Pseudomonas aeruginosa* PAO1. Mol. Microbiol. *17*, 333–343.
8. Davies, D.G., Parsek, M.R., Pearson, J.P., Iglewski, B.H., Costerton, J.W., and Greenberg, E.P. (1998). The involvement of cell-to-cell signals in the development of a bacterial biofilm. Science *280*, 295–298.
9. Winson, M.K., Camara, M., Latifi, A., Foglino, M., Chhabra, S.R., Daykin, M., Bally, M., Chapon, V., Salmond, G.P., and Bycroft, B.W. (1995). Multiple N-acyl-L-homoserine lactone signal molecules regulate production of virulence determinants and secondary metabolites in *Pseudomonas aeruginosa*. Proc. Natl. Acad. Sci. USA *92*, 9427–9431.
10. Brint, J.M., and Ohman, D.E. (1995). Synthesis of multiple exoproducts in *Pseudomonas aeruginosa* is under the control of RhlR-RhlI, another set of regulators in strain PAO1 with homology to the autoinducer-responsive LuxR-LuxI family. J. Bacteriol. *177*, 7155–7163.
11. Albus, A.M., Pesci, E.C., Runyen-Janecky, L.J., West, S.E., and Iglewski, B.H. (1997). Vfr controls quorum sensing in *Pseudomonas aeruginosa*. J. Bacteriol. *179*, 3928–3935.
12. Bottomley, M.J., Muraglia, E., Bazzo, R., and Carfi, A. (2007). Molecular insights into quorum sensing in the human pathogen *Pseudomonas aeruginosa* from the structure of the virulence regulator LasR bound to its autoinducer. J. Biol. Chem. *282*, 13592–13600.
13. Gilbert, K.B., Kim, T.H., Gupta, R., Greenberg, E.P., and Schuster, M. (2009). Global position analysis of the *Pseudomonas aeruginosa* quorum-sensing transcription factor LasR. Mol. Microbiol. *73*, 1072–1085.
14. Schuster, M., and Greenberg, E.P. (2006). A network of networks: quorum-sensing gene regulation in *Pseudomonas aeruginosa*. Int. J. Med. Microbiol. *296*, 73–81.
15. Schuster, M., Lostroh, C.P., Ogi, T., and Greenberg, E.P. (2003). Identification, timing, and signal specificity of *Pseudomonas aeruginosa* quorum-controlled genes: a transcriptome analysis. J. Bacteriol. *185*, 2066–2079.
16. Asfahl, K.L., Smalley, N.E., Chang, A.P., and Dandekar, A.A. (2022). Genetic and transcriptomic characteristics of RhlR-dependent quorum sensing in cystic fibrosis isolates of *Pseudomonas aeruginosa*. mSystems *7*, e0011322.
17. Lee, J., and Zhang, L. (2015). The hierarchy quorum sensing network in *Pseudomonas aeruginosa*. Protein Cell *6*, 26–41. https://doi.org/10.1007/s13238-014-0100-x.
18. McGrath, S., Wade, D.S., and Pesci, E.C. (2004). Dueling quorum sensing systems in *Pseudomonas aeruginosa* control the production of the *Pseudomonas* quinolone signal (PQS). FEMS Microbiol. Lett. *230*, 27–34. https://doi.org/10.1016/S0378-1097(03)00849-8.
19. Rampioni, G., Pustelny, C., Fletcher, M.P., Wright, V.J., Bruce, M., Rumbaugh, K.P., Heeb, S., Cámara, M., and Williams, P. (2010). Transcriptomic analysis reveals a global alkyl-quinolone-independent regulatory role for PqsE in facilitating the environmental adaptation of *Pseudomonas aeruginosa* to plant and animal hosts. Environ. Microbiol. *12*, 1659–1673.
20. Gallagher, L.A., McKnight, S.L., Kuznetsova, M.S., Pesci, E.C., and Manoil, C. (2002). Functions required for extracellular quinolone signaling by *Pseudomonas aeruginosa*. J. Bacteriol. *184*, 6472–6480.
21. Wade, D.S., Calfee, M.W., Rocha, E.R., Ling, E.A., Engstrom, E., Coleman, J.P., and Pesci, E.C. (2005). Regulation of *Pseudomonas* quinolone signal synthesis in *Pseudomonas aeruginosa*. J. Bacteriol. *187*, 4372–4380. https://doi.org/10.1128/JB.187.13.4372-4380.2005.
22. Déziel, E., Gopalan, S., Tampakaki, A.P., Lépine, F., Padfield, K.E., Saucier, M., Xiao, G., and Rahme, L.G. (2005). The contribution of MvfR to *Pseudomonas aeruginosa* pathogenesis and quorum sensing circuitry regulation: multiple quorum sensing-regulated genes are modulated without affecting *lasRI*, *rhlRI* or the production of N-acyl- l-homoserine lactones. Mol. Microbiol. *55*, 998–1014.
23. Farrow, J.M., 3rd, Sund, Z.M., Ellison, M.L., Wade, D.S., Coleman, J.P., and Pesci, E.C. (2008). PqsE functions independently of PqsR-*Pseudomonas* quinolone signal and enhances the rhl quorum-sensing system. J. Bacteriol. *190*, 7043–7051.
24. Zender, M., Witzgall, F., Drees, S.L., Weidel, E., Maurer, C.K., Fetzner, S., Blankenfeldt, W., Empting, M., and Hartmann, R.W. (2016). Dissecting the multiple roles of PqsE in *Pseudomonas aeruginosa* virulence by discovery of small tool compounds. ACS Chem. Biol. *11*, 1755–1763.
25. Drees, S.L., and Fetzner, S. (2015). PqsE of *Pseudomonas aeruginosa* acts as pathway-specific thioesterase in the biosynthesis of alkylquinolone signaling molecules. Chem. Biol. *22*, 611–618.
26. Déziel, E., Lépine, F., Milot, S., He, J., Mindrinos, M.N., Tompkins, R.G., and Rahme, L.G. (2004). Analysis of *Pseudomonas aeruginosa* 4-hydroxy-2-alkylquinolines (HAQs) reveals a role for 4-hydroxy-2-heptylquinoline in cell-to-cell communication. Proc. Natl. Acad. Sci. USA *101*, 1339–1344.
27. Brouwer, S., Pustelny, C., Ritter, C., Klinkert, B., Narberhaus, F., and Häussler, S. (2014). The PqsR and RhlR transcriptional regulators determine the level of *Pseudomonas* quinolone signal synthesis in *Pseudomonas aeruginosa* by producing two different *pqsABCDE* mRNA Isoforms. J. Bacteriol. *196*, 4163–4171. https://doi.org/10.1128/JB.02000-14.
28. Taylor, I.R., Paczkowski, J.E., Jeffrey, P.D., Henke, B.R., Smith, C.D., and Bassler, B.L. (2021). Inhibitor mimetic mutations in the *Pseudomonas aeruginosa* PqsE enzyme reveal a protein–protein interaction with the quorum-sensing receptor RhlR that is vital for virulence factor production. ACS Chem. Biol. *16*, 740–752.
29. Simanek, K.A., Taylor, I.R., Richael, E.K., Lasek-Nesselquist, E., Bassler, B.L., and Paczkowski, J.E. (2022). The PqsE-RhlR interaction regulates RhlR DNA binding to control virulence factor production in *Pseudomonas aeruginosa*. Microbiol. Spectr. *10*, e0210821.
30. Mukherjee, S., Moustafa, D., Smith, C.D., Goldberg, J.B., and Bassler, B.L. (2017). The RhlR quorum-sensing receptor controls *Pseudomonas aeruginosa* pathogenesis and biofilm development independently of its canonical homoserine lactone autoinducer. PLoS Pathog. *13*, e1006504.
31. Mukherjee, S., Moustafa, D.A., Stergioula, V., Smith, C.D., Goldberg, J.B., and Bassler, B.L. (2018). The PqsE and RhlR proteins are an autoinducer synthase-receptor pair that control virulence and biofilm development in *Pseudomonas aeruginosa*. Proc. Natl. Acad. Sci. USA *115*, E9411–E9418.
32. Letizia, M., Mellini, M., Fortuna, A., Visca, P., Imperi, F., Leoni, L., and Rampioni, G. (2022). PqsE expands and differentially modulates the RhlR quorum sensing regulon in *Pseudomonas aeruginosa*. Microbiol. Spectr. *10*, e0096122. https://doi.org/10.1128/spectrum.00961-22.

Please cite this article in press as: Feathers et al., Structure of the RhlR-PqsE complex from *Pseudomonas aeruginosa* reveals mechanistic insights into quorum-sensing gene regulation, Structure (2022), https://doi.org/10.1016/j.str.2022.10.008

33. Wang, Y., Gao, L., Rao, X., Wang, J., Yu, H., Jiang, J., Zhou, W., Wang, J., Xiao, Y., Li, M., et al. (2018). Characterization of lasR-deficient clinical isolates of *Pseudomonas aeruginosa*. Sci. Rep. *8*, 13344.

34. Soto-Aceves, M.P., Cocotl-Yañez, M., Servín-González, L., and Soberón-Chávez, G. (2020). The Rhl quorum-sensing system is at the top of the regulatory hierarchy under phosphate-limiting conditions in *Pseudomonas aeruginosa* PAO1. J. Bacteriol. *203* 004755-20.

35. McKnight, S.L., Iglewski, B.H., and Pesci, E.C. (2000). The *Pseudomonas* quinolone signal regulates rhl quorum sensing in *Pseudomonas aeruginosa*. J. Bacteriol. *182*, 2702–2708. https://doi.org/10.1128/JB.182.10.2702-2708.2000.

36. Groleau, M.-C., de Oliveira Pereira, T., Dekimpe, V., and Déziel, E. (2020). PqsE is essential for RhlR-dependent quorum sensing regulation in *Pseudomonas aeruginosa*. mSystems. 001944-20. https://doi.org/10.1128/msystems.00194-20.

37. McCready, A.R., Paczkowski, J.E., Cong, J.-P., and Bassler, B.L. (2019). An autoinducer-independent RhlR quorum-sensing receptor enables analysis of RhlR regulation. PLoS Pathog. *15*, e1007820.

38. O'Loughlin, C.T., Miller, L.C., Siryaporn, A., Drescher, K., Semmelhack, M.F., and Bassler, B.L. (2013). A quorum-sensing inhibitor blocks *Pseudomonas aeruginosa* virulence and biofilm formation. Proc. Natl. Acad. Sci. USA *110*, 17981–17986.

39. Kim, T., Duong, T., Wu, C.a., Choi, J., Lan, N., Kang, S.W., Lokanath, N.K., Shin, D., Hwang, H.Y., and Kim, K.K. (2014). Structural insights into the molecular mechanism of *Escherichia coli* SdiA, a quorum-sensing receptor. Acta Crystallogr. D Biol. Crystallogr. *70*, 694–707.

40. Zhang, R.G., Pappas, K.M., Pappas, T., Brace, J.L., Miller, P.C., Oulmassov, T., Molyneaux, J.M., Anderson, J.C., Bashkin, J.K., Winans, S.C., and Joachimiak, A. (2002). Structure of a bacterial quorum-sensing transcription factor complexed with pheromone and DNA. Nature *417*, 971–974.

41. Paczkowski, J.E., McCready, A.R., Cong, J.P., Li, Z., Jeffrey, P.D., Smith, C.D., Henke, B.R., Hughson, F.M., and Bassler, B.L. (2019). An autoinducer analogue reveals an alternative mode of ligand binding for the LasR quorum-sensing receptor. ACS Chem. Biol. *14*, 378–389.

42. Glaser, F., Pupko, T., Paz, I., Bell, R.E., Bechor-Shental, D., Martz, E., and Ben-Tal, N. (2003). ConSurf: identification of functional regions in proteins by surface-mapping of phylogenetic information. Bioinformatics *19*, 163–164.

43. Landau, M., Mayrose, I., Rosenberg, Y., Glaser, F., Martz, E., Pupko, T., and Ben-Tal, N. (2005). ConSurf 2005: the projection of evolutionary conservation scores of residues on protein structures. Nucleic Acids Res. *33*, W299–W302.

44. Ashkenazy, H., Abadi, S., Martz, E., Chay, O., Mayrose, I., Pupko, T., and Ben-Tal, N. (2016). ConSurf 2016: an improved methodology to estimate and visualize evolutionary conservation in macromolecules. Nucleic Acids Res. *44*, W344–W350.

45. Celniker, G., Nimrod, G., Ashkenazy, H., Glaser, F., Martz, E., Mayrose, I., Pupko, T., and Ben-Tal, N. (2013). ConSurf: using evolutionary data to raise testable hypotheses about protein function. Isr. J. Chem. *53*, 199–206.

46. Chen, G., Swem, L.R., Swem, D.L., Stauff, D.L., O'Loughlin, C.T., Jeffrey, P.D., Bassler, B.L., and Hughson, F.M. (2011). A strategy for antagonizing quorum sensing. Mol. Cell *42*, 199–209.

47. Feklístov, A., Sharon, B.D., Darst, S.A., and Gross, C.A. (2014). Bacterial sigma factors: a historical, structural, and genomic perspective. Annu. Rev. Microbiol. *68*, 357–376.

48. Taylor, I., R., Jeffrey, P., D., Moustafa, D., A., Goldberg, J., B., and Bassler, B., L. (2022). The PqsE active site as a target for small molecule antimicrobial agents against *Pseudomonas aeruginosa*. Biochemistry *61*, 1894–1903. https://doi.org/10.1101/2022.04.21.489002.

49. Herzik, M.A., Wu, M., and Lander, G.C. (2017). Achieving better-than-3-Å resolution by single-particle cryo-EM at 200 keV. Nat. Methods *14*, 1075–1078.

50. Herzik, M.A., Wu, M., and Lander, G.C. (2019). High-resolution structure determination of sub-100 kDa complexes using conventional cryo-EM. Nat. Commun. *10*, 1032.

51. Mastronarde, D.N. (2005). Automated electron microscope tomography using robust prediction of specimen movements. J. Struct. Biol. *152*, 36–51.

52. Schorb, M., Haberbosch, I., Hagen, W.J.H., Schwab, Y., and Mastronarde, D.N. (2019). Software tools for automated transmission electron microscopy. Nat. Methods *16*, 471–477.

53. Punjani, A., Rubinstein, J., Fleet, D., and Brubaker, M.A. (2017). cryoSPARC: algorithms for rapid unsupervised cryo-EM structure determination. Nat Methods *14*, 290–296. https://doi.org/10.1038/nmeth.4169.

54. Zivanov, J., Nakane, T., and Scheres, S.H.W. (2020). Estimation of high-order aberrations and anisotropic magnification from cryo-EM data sets in {\it RELION}-3.1. IUCrJ *7*, 253–267.

55. Zivanov, J., Nakane, T., Forsberg, B.O., Kimanius, D., Hagen, W.J., Lindahl, E., and Scheres, S.H. (2018). New tools for automated high-resolution cryo-EM structure determination in RELION-3. Elife *7*, e42166.

56. Morin, A., Eisenbraun, B., Key, J., Sanschagrin, P.C., Timony, M.A., Ottaviano, M., and Sliz, P. (2013). Collaboration gets the most out of software. Elife *2*, e01456.

57. Zheng, S.Q., Palovcak, E., Armache, J.P., Verba, K.A., Cheng, Y., and Agard, D.A. (2017). MotionCor2: anisotropic correction of beam-induced motion for improved cryo-electron microscopy. Nat. Methods *14*, 331–332.

58. Zhang, Z., Zhang, T., Wang, S., Gong, Z., Tang, C., Chen, J., and Ding, J. (2014). Molecular mechanism for rabex-5 GEF activation by rabaptin-5. Elife *3*, e02687.

59. Asarnow, D., Palovcak, E., and Cheng, Y. (2019). asarnow/pyem: UCSF pyem v0.5. https://doi.org/10.5281/ZENODO.3576630.

60. Bepler, T., Morin, A., Rapp, M., Brasch, J., Shapiro, L., Noble, A.J., and Berger, B. (2019). Positive-unlabeled convolutional neural networks for particle picking in cryo-electron micrographs. Nat Methods *16*, 1153–1160. https://doi.org/10.1038/s41592-019-0575-8.

61. Liebschner, D., Afonine, P.V., Baker, M.L., Bunkóczi, G., Chen, V.B., Croll, T.I., Hintze, B., Hung, L.W., Jain, S., McCoy, A.J., et al. (2019). Macromolecular structure determination using X-rays, neutrons and electrons: recent developments in {\it Phenix. Acta Crystallogr. D Struct. Biol. *75*, 861–877.

62. Terwilliger, T.C., Ludtke, S.J., Read, R.J., Adams, P.D., and Afonine, P.V. (2020). Improvement of cryo-EM maps by density modification. Nat. Methods *17*, 923–927.

63. Oke, M., Carter, L.G., Johnson, K.A., Liu, H., McMahon, S.A., Yan, X., Kerou, M., Weikart, N.D., Kadi, N., Sheikh, M.A., et al. (2010). The scottish structural proteomics facility: targets, methods and outputs. J. Struct. Funct. Genomics *11*, 167–180.

64. Jumper, J., Evans, R., Pritzel, A., Green, T., Figurnov, M., Ronneberger, O., Tunyasuvunakool, K., Bates, R., Žídek, A., Potapenko, A., et al. (2021). Highly accurate protein structure prediction with AlphaFold. Nature *596*, 583–589.

65. Emsley, P., Lohkamp, B., Scott, W.G., and Cowtan, K. (2010). Features and development of Coot. Acta Crystallogr. D Biol. Crystallogr. *66*, 486–501.

66. Afonine, P.V., Klaholz, B.P., Moriarty, N.W., Poon, B.K., Sobolev, O.V., Terwilliger, T.C., Adams, P.D., and Urzhumtsev, A. (2018). New tools for the analysis and validation of cryo-EM maps and atomic models. Acta Crystallogr. D Struct. Biol. *74*, 814–840.

Please cite this article in press as: Feathers et al., Structure of the RhlR-PqsE complex from *Pseudomonas aeruginosa* reveals mechanistic insights into quorum-sensing gene regulation, Structure (2022), https://doi.org/10.1016/j.str.2022.10.008

STAR★METHODS

KEY RESOURCES TABLE

REAGENT or RESOURCE	SOURCE	IDENTIFIER
Bacterial and virus strains		
Strains used in this study are listed in Table S2	This paper	N/A
Chemicals, peptides, and recombinant proteins		
Meta-bromo-thiolactone (mBTL)	Synthesized by Wuxi AppTec, gift from the Bassler lab (McCready et al.[1])	N/A
Isopropyl-β-D-thiogalactopyranoside	GoldBio	CAS #: 367-93-1
N-butyryl-L-homoserine lactone (C_4HSL)	Cayman Chemical	Item #: 10007898
N-(3-oxododecanoyl)-L-homoserine lactone ($3OC_{12}$HSL)	Cayman Chemical	Item #: 10007895
L-arabinose	Millipore Sigma	CAS #: 5328-37-0
Fluorinated Fos-choline-8	Anatrace	Item #: F300F
Critical commercial assays		
SuperScript III Reverse Transcriptase kit	ThermoFisher	Item #: 18080044
SYBR™ Select Master Mix	Applied Biosystems	Item #: 4472903
Deposited data		
PqsE-RhlR:mBTL	This paper	PDB: 8DQ0
PqsE-RhlR:mBTL	This paper	EMD: 27645
PqsE-RhlR:mBTL	This paper	EMPIAR: 11247
PqsE-RhlR:mBTL-DNA	This paper	PDB: 8DQ1
PqsE-RhlR:mBTL-DNA	This paper	EMD: 27646
PqsE-RhlR:mBTL-DNA	This paper	EMPIAR: 1 1247
Experimental models: Organisms/strains		
Pseudomonas aeruginosa: strain UCBPP-PA14	ATCC	BAA-1744
Escherichia coli: strain BL21 (DE3)	New England Biolabs	Item #: C2527H
Oligonucleotides		
Primers used in this study are listed in Table S3	This paper	N/A
Recombinant DNA		
Plasmids used in this study are listed in Table S2	This paper	N/A
Software and algorithms		
SerialEM	Mastronarde,[2] Schorb et al.[3]	https://bio3d.colorado.edu/SerialEM/
cryoSPARC	Punjani et al.[4]	https://cryosparc.com/
MotionCor2	Zheng et al.[5]	https://emcore.ucsf.edu/ucsf-software
RELION	Zivanov et al.[4]	https://relion.readthedocs.io/en/release-4.0/
Phenix	Liebschner et al.[6]	https://phenix-online.org/
Coot	Emsley et al.[7]	https://www2.mrc-lmb.cam.ac.uk/personal/pemsley/coot/
Topaz	Bepler et al.[8]	http://topaz.csail.mit.edu
Other		
300-mesh gold-support grids	Quantifoil	Item #: R1.2/1.3
Ni-NTA resin	Qiagen	Item #: 30210

Please cite this article in press as: Feathers et al., Structure of the RhlR-PqsE complex from *Pseudomonas aeruginosa* reveals mechanistic insights into quorum-sensing gene regulation, Structure (2022), https://doi.org/10.1016/j.str.2022.10.008

CellPress

RESOURCE AVAILABILITY

Lead contact

Further information and requests for resources and reagents should be directed to and will be fulfilled by the lead contact, Jon E. Paczkowski (jon.paczkowski@health.ny.gov).

Materials availability

All unique/stable reagents generated in this study are available from the lead contact without restriction.

Data and code availability

- Structure data for the RhlR-PqsE complex (PDB: 8DQ0; EMD: 27645) and the RhlR-PqsE:DNA (PDB: 8DQ1; EMD: 27646) have been deposited. The raw micrographs have been deposited in the Electron Microscopy Public Image Archive (EMPIAR: 11247).
- This paper does not report original code.
- Any additional information required to reanalyze the data reported in this paper is available from the lead contact upon request.

EXPERIMENTAL MODEL AND SUBJECT DETAILS

P. aeruginosa strain UCBPP-PA14 was used for all experiments related to the study. Strains containing gene deletions were constructed using this background. WT and deletion strains were cultured in LB media (10 g/L tryptone, 10 g/L NaCl, and 5 g/L yeast extract). When necessary to maintain plasmid-borne gene expression in the different genetic backgrounds, LB media was supplemented with 400 μg/μL of carbenicillin. *E. coli* strain BL21 (DE3) and TOP10 (New England Biolabs) were used for protein expression and luciferase production assays, respectively. All *E. coli* strains were cultured in LB media containing the appropriate antibiotics. Ampicillin was used at 100 μg/μL, kanamycin was used at 50 μg/μL, and tetracycline was used at 100 μg/μL. See Tables S2 and S3 for strain-specific details.

METHOD DETAILS

Plasmid and strain construction

Plasmids and strains were constructed using standard molecular cloning techniques. Specifically, we note that the RhlR overexpression construct was not tagged at the N-terminus, as a tag in this region of the protein prevented RhlR binding to PqsE. We did not specifically test RhlR overexpression constructs tagged at the C-terminus due to the potential that a tag in this region of RhlR would disrupt functional protein-DNA interactions. PqsE constructs tagged at the N-terminus were previously shown to be functional *in vivo*[31] indicating that it has no effect on the ability of PqsE to bind to RhlR. Table S2 lists the plasmids and strains used in the study. Table S3 lists the primers used in the study.

Affinity purification pulldown

Overnight cultures of *E. coli* strains carrying overexpression vectors for producing variants of 6x-His-PqsE or RhlR proteins were diluted 1:100 and grown at 37°C with shaking to an OD600 = 1.0. Protein production was induced by the addition of 1 mM isopropyl-β-D-thiogalactopyranoside (IPTG). 100 μM mBTL was added to the strains producing RhlR. After 4 h, cells were pelleted by centrifugation at 10,000 x *g* at 4°C for 30 min and the pellets were frozen until lysis. Lysis buffer (50 mM Tris-HCl [pH 8.0], 150 mM NaCl, 20 mM imidazole) was added in proportion to the pellet size (250 μL/25 mL culture). Resuspended pellets were transferred to microcentrifuge tubes and lysed via sonication, followed by centrifugation at 15,000 x *g* at 4°C for 20 min. Equal amounts of supernatant fractions from PqsE- and RhlR-containing cells were combined, with 20 μL saved for input assessment. Promega MagneHis™ Ni-Particles, (20 μL and 40 μL per sample for PqsE variants and RhlR variants, respectively) were washed with lysis buffer and resuspended in lysis buffer at 100 μL/sample, followed by mixing with the above protein samples for 1.5 h at 4°C with inversion. Samples were subjected to brief centrifugation at 250 x *g*, placed on a magnetic rack, and the clarified supernatants aspirated. Samples were washed three times with lysis buffer and 6x-His-protein was eluted with two washes of 20 μL of elution buffer (50 mM Tris-HCl [pH 8.0], 150 mM NaCl, 500 mM imidazole). Eluted protein was mixed 1:1 with 2x sample buffer and loaded onto SDS-PAGE gels. Gels were stained with Coomassie brilliant blue and imaged on a Bio-Rad EZ-Doc gel imager.

E. coli light assay

pqsE and *rhlR* were expressed from the *lac* promoter and the pBAD promoter, respectively, in an *E. coli* strain containing the p*rhlA-luxCDABE* fusion. The protocol has been described previously.[29] Overnight cultures of *E. coli* strains harboring plasmids with *rhlR* or *rhlR* mutants driven by the pBAD promoter, *luxCDABE* under the p*rhlA* promoter, and either the pACYC184 vector or pACYC184 harboring WT *pqsE* were grown from single colonies at 37°C in LB medium supplemented with ampicillin, kanamycin, and tetracycline. The overnight cultures were diluted 1:100 into fresh LB medium containing antibiotics and 0.1% arabinose and added to the wells of a black, clear-bottomed 96-well plate at 200 μL per well. C_4HSL (Cayman Chemical) was supplied at 1 μM. Plates were incubated for 4 h at 37°C with shaking. Dose response assays were performed as described previously, with a top concentration of 10 μM in 2-fold serial dilutions.

Please cite this article in press as: Feathers et al., Structure of the RhlR-PqsE complex from *Pseudomonas aeruginosa* reveals mechanistic insights into quorum-sensing gene regulation, Structure (2022), https://doi.org/10.1016/j.str.2022.10.008

Pyocyanin production assay

Pyocyanin was measured as described previously with some modifications. Briefly, overnight cultures were started from freezer stocks in 3 mL LB media with carbenicillin (400 μg/mL) for strains harboring *pqsE* or *rhlR* variant genes on the pUCP18 plasmid. The OD_{600} was measured using a 1:10 dilution of each culture in LB media. 1 mL of each overnight culture was pelleted, and the supernatant transferred to a cuvette. Pyocyanin readings were measured at OD_{695}. The OD_{695} for each culture was normalized to growth (OD_{600}) and pyocyanin production was graphed as a percentage of the WT value.

RNA extraction and qRT-PCR

500 ng of DNA-depleted mRNA was incubated with 1 μL random hexamers (Integrated DNA Technologies) and 1 μL 10mM dNTPs at 65°C for 5 min in a total reaction volume of 13 μL. The reactions were chilled on ice for 2 min. cDNA was prepared with a SuperScript III Reverse Transcriptase kit (Invitrogen) in total reaction volumes of 20 μL. SYBR Select Master Mix (Applied Biosystems) was used for RT-PCR. Briefly, 2x SYBR Select was mixed with primers at 200 nM final concentration and 18 μL were aliquoted per well. Finally, 20-μL cDNA reactions were diluted 1:5 and 2 μL added per well. A 7500 Fast real-time PCR system (Applied Biosystems) and software (v2.3) were used for cycle threshold quantification and relative gene expression analysis.

Protein purification and cryo-EM sample preparation

The RhlR-PqsE complex was expressed and purified using a similar method as the affinity chromatography pulldown with some modifications. Approximately 4 L of cells expressing RhlR in the presence of 100 μM mBTL were grown for every 1 L of cells expressing 6x-His-PqsE. As in the pulldown, the separate cell lysates were combined. Subsequently, the lysates were incubated with Ni-NTA resin (Qiagen) and eluted using 500 mM imidazole in lysis buffer. Fractions containing the RhlR-PqsE complex were pooled and concentrated. Concentrated protein was then run on a Superdex-200 column equilibrated in 150 mM NaCl and 20 mM Tris-HCl pH 8.0. Peak fractions were pooled and concentrated to 5 mg/mL at which point the complex was incubated with 22 bp duplex DNA for 30 min at RT. Fluorinated Fos-choline-8 (Anatrace) was added to the reaction to a final concentration of 2 mM and flash frozen in lN_2. Aliquots of PqsE-RhlR-DNA complex were stored at −80°C and thawed immediately before vitrification. 3 μL of the protein solution was applied to Quantifoil R1.2/1.3 300-mesh gold-support grids that had been glow-discharged for 60 seconds at 15 mA in a Pelco EasiGlo instrument. Following a 10 second wait time, grids were blotted for 3 seconds with blot force 0 at 4°C and 100% humidity and immediately plunge frozen in liquid ethane using a FEI Mark IV Vitrobot.

Imaging conditions

Cryo-EM data collection was performed using a Thermo Fisher Scientific Talos Arctica operated at 200 keV equipped with a Gatan K3 detector operated in counting mode with 0.5X-binning (super-resolution mode) and a Gatan BioQuantum energy filter with a slit width of 20 eV.

Microscope alignments were performed on a gold diffraction cross-grating following published procedures for a 2-condenser instrument.[49,50] Parallel conditions were determined in diffraction mode at the imaging magnification. A 50 μm C2 aperture size was chosen, and the spot size was set so that the dose rate at the detector was ~25 e^-/physical pixel/sec over vacuum. A 100 μm objective aperture was used during data collection.

SerialEM[51,52] was used for automated data collection of 60 frame fractionated exposures with a total dose of ~50 $e^-/Å^2$ so that the dose per frame was ~0.8 $e-/Å^2$. Beam-image shift was used to collect 9 movies per stage per stage movement at defocus values ranging from −0.8 μm to −1.5 μm with a nominal magnification of 63,000 resulting in a physical pixel size of 1.29Å.

Data processing

All cryo-EM data processing was performed within cryoSPARC[53] and RELION 3.1 or RELION 4.0[54,55] and software was maintained by SBGrid.[56] Frames from 2357 movies were aligned and dose-weighted with MotionCor2.[57] Defocus values were calculated for the motion-corrected micrographs with GCTF[58] in RELION. Initially, roughly 1100 particles were manually picked and 2D classified in RELION to generate 2D templates for autopicking. 3,065,247 particles Fourier cropped to 2.58Å/pix were extracted and imported into cryoSPARC. A subset of 776 motion-corrected micrographs was imported into cryoSPARC and processed in parallel by performing blob-picking and multiple rounds of 2D classification followed by a 3-class *ab initio* reconstruction and hetero refinement resulting in a map with an estimated resolution of 5.58 Å. This map was used as a 3D reference model along with 2 junk classes to sort the particle set imported from RELION resulting in a class of 1,501,800 particles that refined to an estimated resolution of 6.14Å. The particles from cryoSPARC were exported back to RELION using pyem.[59] Single-class 3D classification was performed initially followed by iterative rounds of 3D autorefinement and CTF refinement which produced a reconstruction with 4.42 Å estimated resolution. Bayesian polishing followed by an additional round of 3D autorefinement and CTF refinement did not result in an improved resolution estimate. Fixed angle 3D classification of the polished refined particles split 858,871 into a single class that was subjected to further iterations of 3D classification, 3D autorefinement and CTF refinement. The final particle set containing 40,761 particles resulted in a reconstruction with an estimated resolution of 3.74 Å.

To determine the structure of the DNA-bound complex, the stack containing 1,501,800 polished refined particles was 3D classified and refined until a class of 232,670 particles with additional density resembling DNA was evident. These particles were further classified and refined resulting in a 6.37 Å reconstruction of the complex with DNA. The 49,109 particles with DNA were used to train a Topaz model in RELION 4.0 that subsequently picked 950,125 particles from the original 2357 micrographs.[60] Processing of the

Topaz picked particles was carried similar to before with the addition of a focused mask around the DNA density for fixed angle 3D classifications in the later stages of classification. The final particle set for the complex consisted of 84,842 images that produced a reconstruction with an estimated resolution of 4.1 Å.

Model building

Maps were postprocessed in Phenix[61] using the cryo-EM density modification module.[62] A preliminary model was generated by docking the PqsE crystal structure (PDB: 2VW8[63]) and the predicted RhlR structure[64] into the density modified cryo-EM map. Iterative cycles of manual rebuilding in Coot[65] and real space refinement in Phenix[66] were then performed. The 3D reconstruction of RhlR-PqsE bound to DNA was lower resolution, but the major and minor grooves were clearly resolved in the map. We assigned nucleotide residues taking into account the symmetry of the DBD domain relative to the DNA and the highly conserved bases of the proposed consensus sequence in the *rhl* box. See Table 1 for cryo-EM data collection, processing, and model validation details.

QUANTIFICATION AND STATISTICAL ANALYSIS

Affinity pulldown experiments shown in Figure 2 were quantified in Figure S4 using ImageJ. All data depicted as graphs in this paper were created using GraphPad Prism 9. Statistical analyses were performed using GraphPad Prism 9. Details pertaining to each statistical analysis are provided in the corresponding figure legend, including the statistical tests performed, the number of samples used, and the relevant precision measures.